

Research Article

Loosely Formation-Displaced Geostationary Orbit Optimization with Complex Hybrid Sail Propulsion

Yuan Liu,¹ Yong Hao,¹ and Weiwei Liu² 

¹College of Automation, Harbin Engineering University, Harbin 150001, China

²School of Economics and Management, Harbin Engineering University, Harbin 150001, China

Correspondence should be addressed to Weiwei Liu; heulww@163.com

Received 23 March 2018; Revised 16 April 2018; Accepted 8 May 2018; Published 6 June 2018

Academic Editor: Yimin Zhou

Copyright © 2018 Yuan Liu et al. This is an open access article distributed under the Creative Commons Attribution License, which permits unrestricted use, distribution, and reproduction in any medium, provided the original work is properly cited.

To explore the performance of hybrid sail and overcome the congestion of geostationary orbit, this work proposes a method intended to optimize the trajectories of the spacecraft formation and extend the concept of displaced geostationary orbit by loosening the relative distance and introducing a station-keeping box. The multispacecraft formation is a typical complex system with nonlinear dynamics, and the hybrid propulsion system introduces additional complexity. To solve this problem, suboptimal trajectories with constant relative distance constraints are first found with inverse methods, which were referred to as ideal displaced geostationary orbits. Then, the suboptimal trajectories are used as a first guess for a direct optimization algorithm based on Gauss pseudospectral algorithm, which loosens the relative distance constraints and allows the spacecraft to be placed anywhere inside the station-keeping box. The optimization results show that the loosely formation and station-keeping box can create more flexible trajectories and achieve higher efficiency of the hybrid sail propulsion system, which can save about 40% propellant consumption.

1. Introduction

The geostationary orbit (GEO) is a circular, equatorial orbit whose period equals the Earth's rotational period, enabling the use of applications, such as telecommunications and geoscience monitoring. The GEO allows a satellite to be stationary above a certain point on the Earth's equator. For this reason, it is a unique and currently congested orbit, especially at longitudes above densely populated areas [1]. To ease the congestion of the GEO slot, the concept of replacing the GEO with a non-Keplerian orbit (NKO) has been proposed [2].

The NKOs are spacecraft trajectories which can be achieved by a continuous control acceleration, and McKay et al. gave comprehensive introduction about NKOs in a survey [3]. However, continuous propulsion is necessary for NKO maintenance, and it can be provided either by a solar electric propulsion (SEP) thruster [4] or by a hybrid of SEP and solar sailing [5].

Solar sailing demands many high-technology requirements on materials, control, and structures [6]. Recently, several solar sail demonstrator missions have been achieved with Japan Aerospace Exploration Agency (JAXA), the Interplanetary Kite-Craft Accelerated by Radiation of the Sun (IKAROS), National Aeronautics and Space Administration (NASA), NanoSail-D2, and the Planetary Society, LightSail 1 [7–9]. For NKOs, there have been some solid conclusions that adding the propulsion-saving propellant such as solar sails is helpful to reduce the propellant consumption, which ensures a longer mission lifetime [5].

Previous works proposed that there be possibility of combining a relatively small sail and SEP, which will be more feasible than equipping a big sail for a near-term spacecraft [5, 10–12]. Guided by this concept, several researches have been done to enhance the overall performance of the hybrid propulsion system, especially to minimize the long-term propellant consumption for Earth pole-sitter [5] and other planets' pole-sitter [13], transferring from Earth to

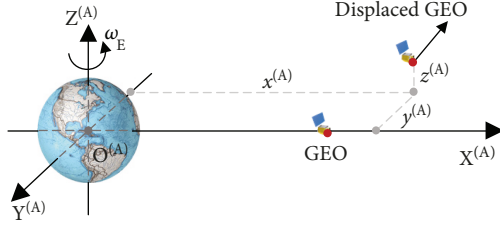


FIGURE 1: Displaced GEO in the rotating reference frame (A).

other planets [14, 15] and from north/south to south/north pole-sitter orbits [11]. According to those studies, the hybrid sail is an effective solution for the long-term NKO maintenance, which has better performance on propellant consumption than pure SEP and less complexity than a large sail.

The displaced GEO through solar radiation pressure was first shown to be feasible by Baig and McInnes [16]. After that, Heiligers et al. [1, 2] have demonstrated that the hybrid sail-displaced GEO is more feasible with strict position constraints. Then, Arnot et al. proposed that new families of relative orbits for spacecraft formation flight will be generated by applying continuous thrust with minimal intervention in the dynamics of the problem [17].

However, we believe that loosening the formation relative distance constraints is helpful to release the potential of hybrid sail. In this paper, we extend the previous works by keeping several spacecrafts in an assigned station-keeping box with loosely formation. The concept of a station-keeping box is found to have the drawback that the spacecraft does not always have constant relative position with respect to an Earth observer; it is not truly “geo-stationary”. Yet, if the station-keeping box is small enough, the negative effects of pointing problems can be restricted to an acceptable level so that this displacement will not be perceivable from the Earth.

The structure of this paper is organized as the following. In Section 2, the system dynamics and the satellite formation model are described. In Section 3, mission profiles for spacecraft strict formation on displaced GEOs are presented and an inverse method to minimize the SEP thrust and obtain the corresponding solar sail control is introduced. In Section 4, the optimization method used to discover the trajectories of loosely formation spacecraft in a station-keeping box to minimize the propellant mass is described.

2. Equations of Motion

The displaced GEO is an NKO whose period equals that of the Earth’s rotation [1]. Compared with the distance from the Sun, a spacecraft in a displaced GEO is much closer to the Earth. Therefore, the dynamics are defined as two-body, Earth-centered dynamics, neglecting perturbations from the higher order harmonics and from the Earth’s potential, the Moon, Sun, and so on. Figure 1 shows a rotating reference frame $A(X^{(A)}, Y^{(A)}, Z^{(A)})$, which is centered at the Earth center, with the $X^{(A)}$ axis pointing towards the slot of an ideal GEO and the $Z^{(A)}$ axis aligning with the angular momentum

vector of the Earth and perpendicular to the equatorial plane. Then, the $Y^{(A)}$ axis completes the right-handed Cartesian reference frame.

The basic idea of displaced GEO spacecraft is that its relative movement with an Earth surface observer can be neglected and its period exactly equals that of the ideal GEO. The equations that describe the dynamics of the spacecraft in the frame (A) are

$$\begin{aligned}\ddot{x}^{(A)} &= 2\omega_e \dot{y}^{(A)} + \omega_e^2 x^{(A)} - \frac{\mu_e x^{(A)}}{r^3} + a_X^{(A)}, \\ \ddot{y}^{(A)} &= -2\omega_e \dot{x}^{(A)} + \omega_e^2 y^{(A)} - \frac{\mu_e y^{(A)}}{r^3} + a_Y^{(A)}, \\ \ddot{z}^{(A)} &= -\frac{\mu_e z^{(A)}}{r^3} + a_Z^{(A)}.\end{aligned}\quad (1)$$

The spacecraft position vector is $\mathbf{r}^{(A)} = [x^{(A)}, y^{(A)}, z^{(A)}]^T$, $r = \|\mathbf{r}^{(A)}\|$, ω_e is the Earth’s constant angular velocity, and μ_e is the gravitational parameter of the Earth. For a hybrid sail propulsion system, the thrust-induced acceleration $\mathbf{a}^{(A)} = [a_X^{(A)}, a_Y^{(A)}, a_Z^{(A)}]^T$ can be written as

$$\mathbf{a}^{(A)} = \mathbf{a}_{\text{SEP}}^{(A)} + \mathbf{a}_S^{(A)}, \quad (2)$$

where $\mathbf{a}_{\text{SEP}}^{(A)}$ is the acceleration of the SEP thruster and $\mathbf{a}_S^{(A)}$ is the acceleration of the solar sail.

$$\begin{aligned}\mathbf{a}_{\text{SEP}}^{(A)} &= \frac{\mathbf{f}_{\text{SEP}}^{(A)}}{m}, \\ \mathbf{a}_S^{(A)} &= \beta_0 \frac{m_0 \mu_s}{m s^2} (\hat{\mathbf{n}}^{(A)} \cdot \hat{\mathbf{s}}^{(A)})^2 \hat{\mathbf{n}}^{(A)},\end{aligned}\quad (3)$$

in which $\mathbf{f}_{\text{SEP}}^{(A)} = [f_X^{(A)} \ f_Y^{(A)} \ f_Z^{(A)}]^T$ is the SEP thrust vector, $f_{\text{SEP}} = \|\mathbf{f}_{\text{SEP}}^{(A)}\|$, and m is the spacecraft mass. Because of the consumption of SEP propellant, m can be profiled as the following:

$$\dot{m} = -\frac{f_{\text{SEP}}}{I_{\text{SP}}} g_0, \quad (4)$$

in which I_{SP} is the specific impulse (we adopt the value of $I_{\text{SP}} = 3200\text{s}$, which can be obtained with current engine technology [12]) and g_0 is the standard Earth surface gravity acceleration.

Furthermore, in this paper, a perfect solar sail force model is used to account for specular reflection, where μ_s is the gravitational parameter of the Sun, $\hat{\mathbf{n}}$ is the vector normal to the sail surface, m_0 is the initial mass at time $t = 0$, \mathbf{s} is the Sun-sail vector, and $\hat{\mathbf{s}}$ is the unit vector along \mathbf{s} . In our work, $\|\mathbf{s}\|$ is approximated by a constant Sun-Earth distance of one astronomical unit (AU). The parameter β_0 indicates the lightness number, the value of $\beta_0 = 0$ is plausible for a near-term mission, and a value of $\beta_0 = 0.1$ for a long-term mission [18]. The unit vectors $\hat{\mathbf{n}}$ and $\hat{\mathbf{s}}$ can be expressed in the easiest way in an auxiliary frame $B(X^{(B)}, Y^{(B)}, Z^{(B)})$ (see Figure 2). The $X^{(B)}$ axis coincides with the Sun-sail vector (neglecting

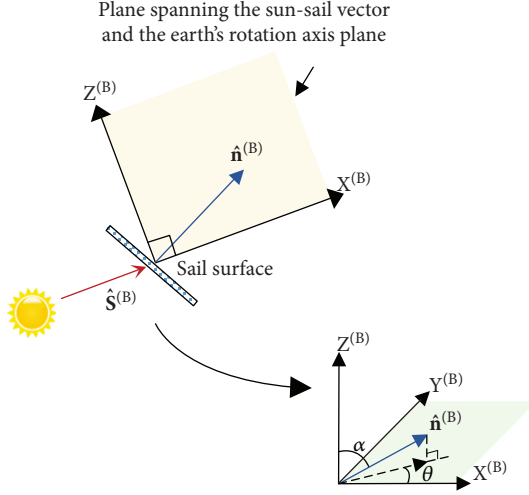


FIGURE 2: Frame (B) with sail normal vector $\hat{\mathbf{n}}$, pitch angle α , and yaw angle θ .

the tiny variation in the direction of the Sun-sail vector over one orbit, assuming it to be aligned with the Sun-Earth vector), the $Z^{(B)}$ axis is perpendicular to the $X^{(B)}$ axis and lies in the plane spanning the Sun-sail vector and the Earth's rotation axis, and the $Y^{(B)}$ axis completes the right-handed reference frame. Using the pitch angle α and yaw angle θ as given in Figure 2, $\hat{\mathbf{n}}$ can be expressed as

$$\hat{\mathbf{n}}^{(B)} = [\sin \alpha \cos \theta \quad \sin \alpha \sin \theta \quad \cos \alpha]^T. \quad (5)$$

Because $\hat{\mathbf{n}}^{(B)}$ should always point away from the Sun, in the frame (B), the following attitude constraints apply:

$$\begin{aligned} 0 &\leq \alpha \leq \pi, \\ -\frac{\pi}{2} &\leq \theta \leq \frac{\pi}{2}. \end{aligned} \quad (6)$$

Using ψ to describe the angle between $\hat{\mathbf{s}}$ and the equatorial plane, which reaches its maximum value (equals the Earth's obliquity to the ecliptic, δ) at winter solstice and reaches its minimum value $-\delta$ at summer solstice, $\hat{\mathbf{s}}^{(B)}$ can be expressed as

$$\hat{\mathbf{s}}^{(B)} = [\cos \psi \quad 0 \quad \sin \psi]^T. \quad (7)$$

The evolution of the displaced spacecraft state $\mathbf{X}^{(A)} = [\mathbf{r}^{(A)} \dot{\mathbf{r}}^{(A)} \mathbf{m}]^T$ can be expressed in the differential form:

$$\dot{\mathbf{X}}^{(A)} = \begin{bmatrix} \dot{\mathbf{r}}^{(A)} \\ \ddot{\mathbf{r}}^{(A)} \\ \dot{m} \end{bmatrix}. \quad (8)$$

We assume that there is one leader and n ($n \geq 1$) followers in each formation. In this paper, we consider a test case of a formation with one leader and two followers, and the details are defined and shown in Table 1.

TABLE 1: Spacecraft parameters.

Parameters	Leader	Follower 1	Follower 2
Initial mass (kg)	1000	900	800
Initial propellant mass (kg)	700	500	550
I_{SP} (s)	3200	3200	3200
β_0	0.2	0.1	0.1

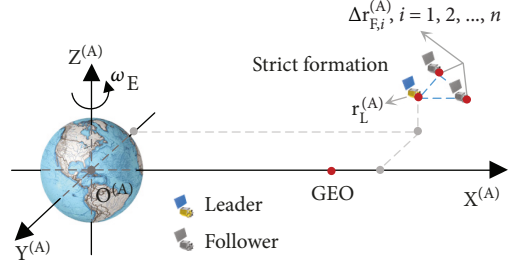


FIGURE 3: Strict formation in the rotating reference frame (A).

3. Strict Formation-Displaced Geostationary Orbits

This section deals with the strict formation-displaced GEO analyses by assuming that the problem is approximated as a formation with each spacecraft in a constant flat non-Keplerian-displaced GEO. The assumption that trajectories and the corresponding controls are used as the first guess for the optimization algorithm will be presented in Section 4.

3.1. Approach. For a strict spacecraft formation, the relative positions between each two agents are always constant (see Figure 3). If one formation is placed on an ideal displaced GEO (which keeps still for the observers on Earth), each spacecraft will be a fixed point in the frame (A). $\mathbf{r}_L^{(A)}$ is the position of the leader, meanwhile, $\Delta \mathbf{r}_{F,i}^{(A)}$ is the relative position of i th follower spacecraft with the leader, and $\dot{\mathbf{r}}_L^{(A)} = \ddot{\mathbf{r}}_L^{(A)} = \Delta \dot{\mathbf{r}}_{F,i}^{(A)} = \Delta \ddot{\mathbf{r}}_{F,i}^{(A)} = 0$. Once the trajectory of every spacecraft is known, the inverse method can be used to find uniquely required accelerations from (8).

For a hybrid propulsion system (both pure SEP, $\beta_0 = 0$, and pure sail, $f_{SEP} = 0$, are special cases), the optimal controls of spacecraft require that the SEP consumes as little propellant as possible, which can be achieved by the following steps:

- (1) Divide one day (Earth's rotation period) into several equal instants.
- (2) Use MATLAB's genetic algorithm toolbox to find the optimal control of solar sail (including the pitch angle α and yaw angle θ) and to minimize the $a_{SEP}^{(A)}$ at each instant.
- (3) Assume that the $a_{SEP}^{(A)}$ remains constant between two adjacent instants and update the m according to the integration of (4).

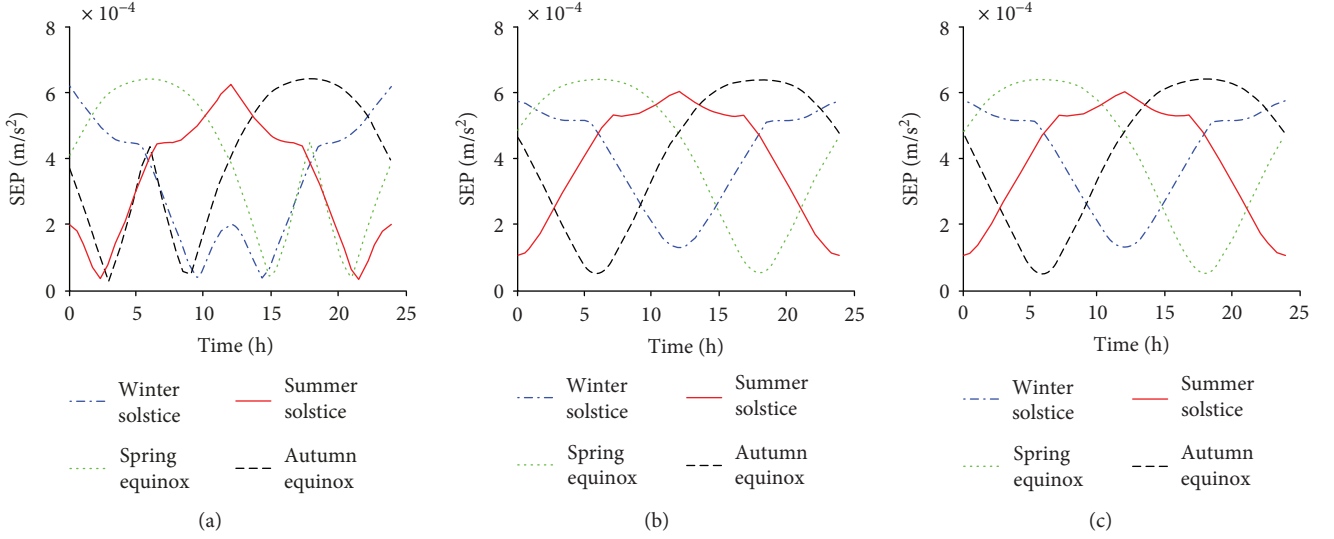


FIGURE 4: Strict formation on ideal displaced GEO for the hybrid sail case: acceleration provided by SEP (a) leader, (b) follower 1, and (c) follower 2 in the frame (A).

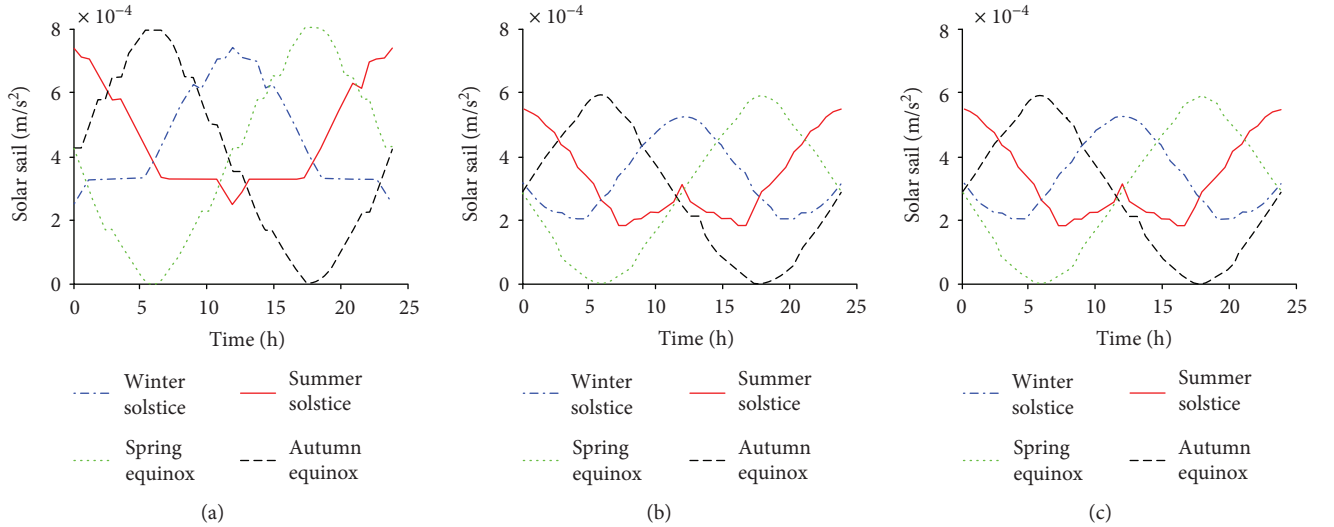


FIGURE 5: Strict formation on ideal displaced GEO for the hybrid sail case: acceleration provided by solar sail (a) leader, (b) follower 1, and (c) follower 2 in the frame (A).

- (4) Repeat steps 1 to 3 until the orbit is complete at the time $t = t_f$, where t_f equals one Earth's rotation period.

3.2. Results. In the test, the spacecraft's positions are defined as $\mathbf{r}_L^{(A)} = [40 \text{ km} + r_{\text{GEO}} 0 \text{ km} 0 \text{ km}]^T$, $\Delta \mathbf{r}_{F,1}^{(A)} = [0 \text{ km} 5 \text{ km} 5 \text{ km}]^T$, $\Delta \mathbf{r}_{F,2}^{(A)} = [0 \text{ km} -5 \text{ km} 5 \text{ km}]^T$, where $\mathbf{r}_L^{(A)} = \mathbf{r}_{F,i}^{(A)} + \Delta \mathbf{r}_{F,i}^{(A)}$ ($i = 1, 2, \dots, n$). In the pure SEP case, the SEP provides the whole acceleration for orbital maintenance. In a relative short period like one day, ignoring the impact of orbit perturbation, the accelerations provided by SEP are constant, which lies at a separation of $6.375 \times 10^{-4} \text{ m/s}^2$ for leader and $6.381 \times 10^{-4} \text{ m/s}^2$ for both followers 1 and 2. As to the hybrid sail case, because the Sun-Earth direction changes with the period of one year,

the accelerations of SEP and solar sail are no longer constant and show symmetrical characteristic on different days with different Sun-Earth directions (see Figures 4 and 5). Obviously, with the help of the solar sail, the SEP provided less acceleration than the pure SEP case at most of the time. This means that a part of propellant is saved, and the spacecraft formation will be maintained for a longer time.

Figure 6 shows the mass of the simulation result. To make the comparison clear, we assume that the spacecraft's parameters are as described in Table 1. In the pure SEP case, the mass of the spacecraft decreased at a constant rate. After one-day formation maintenance, the leader's mass drops from 1000 kg to 998.252 kg, the follower 1's mass drops from 900 kg to 898.425 kg, and the follower 2's mass drops from 800 kg to 798.600 kg. For the hybrid sail case, compared with

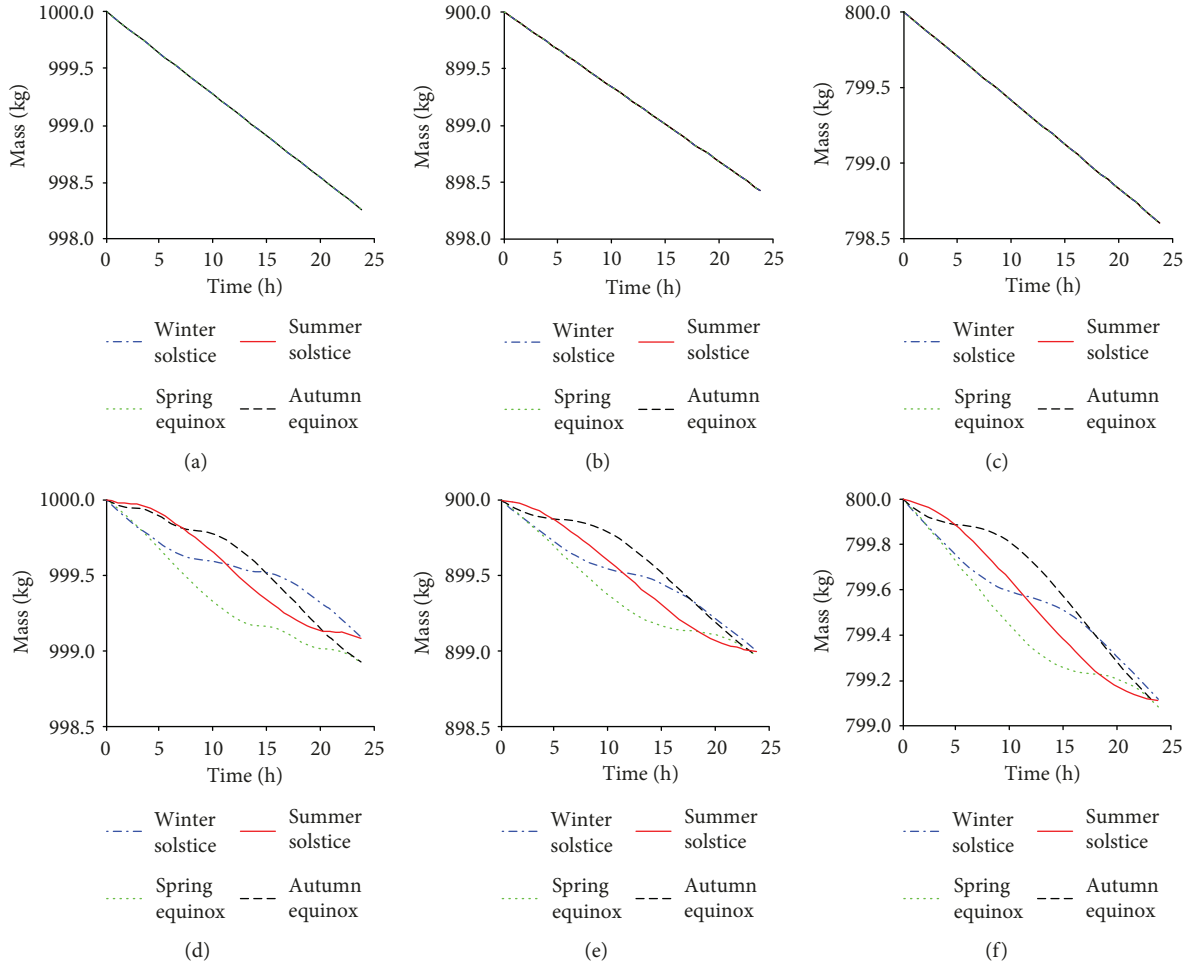


FIGURE 6: Strict formation on ideal displaced GEO: mass of pure SEP (a) leader, (b) follower 1, and (c) follower 2 and mass of hybrid sail (d) leader, (e) follower 1, and (f) follower 2 in the frame (A).

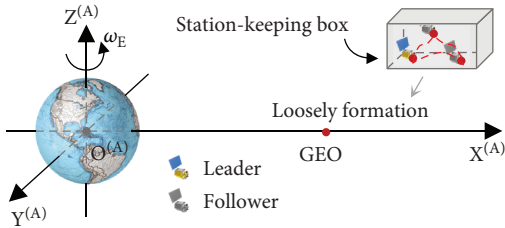


FIGURE 7: Loosely formation in the rotating reference frame (A).

the pure SEP case, significant mass saving is achieved, which proves the effectiveness of hybrid sail on the propellant saving. In the next section, we try to get more mass saving by introducing a station-keeping box and loosening the relative distance constraints between each two spacecrafts.

4. Optimal Loosely Formation-Displaced Geostationary Orbits

For a loosely spacecraft formation, the relative distances between any two agents are variable and are limited to a minimum value of d_{\min} (to avoid collision $d_{\min} > 0$) and to a

maximum value of d_{\max} . The value of $|d_{\max} - d_{\min}|$ is defined as the loosely distance. In addition, to ensure the loosely formation to be nearly geostationary (not truly geostationary) for an Earth observer, the concept of a station-keeping box placed around a real GEO is introduced and all the spacecrafts are required to be in the station-keeping box all the time (see Figure 7). For a loosely spacecraft formation, with loosely relative distance and the station-keeping box, it is possible for the spacecraft to enable propellant optimal trajectories to save more mass. However, because the trajectories of spacecraft are functions of time and the expression of them is unknown, the optimal trajectories cannot be simply obtained with the inverse method. Hence, a method is used to find both optimal trajectories and controls, which minimizes the whole formation's propellant usage and allows the formation to be kept in a displaced GEO.

4.1. Approach. The problem is to find optimal periodic orbits with minimum propellant consumption. Therefore, the cost function can be simply defined as

$$J = - \left[m_L(t_f) + \sum_{i=1}^n m_{F,i}(t_f) \right], \quad (9)$$

that is, to maximize the whole final mass of all spacecrafts after one period (for displaced GOE t_f equals one day). In the frame (A), the leader spacecraft's dynamics can be described as (1), the followers' relative dynamics (with the leader) $\Delta \mathbf{r}_{F,i}^{(A)} = [\Delta x_{F,i}^{(A)}, \Delta y_{F,i}^{(A)}, \Delta z_{F,i}^{(A)}]^T$ ($i = 1, 2, 3, \dots, n$) can be written as

$$\begin{aligned} \Delta \ddot{x}_{F,i}^{(A)} &= \ddot{x}_L^{(A)} - \ddot{x}_{F,i}^{(A)} = 2\omega_e \left(\dot{y}_L^{(A)} - \dot{y}_{F,i}^{(A)} \right) \\ &\quad + \omega_e^2 \left(x_L^{(A)} - x_{F,i}^{(A)} \right) - \mu_e \left(\frac{x_L^{(A)}}{r_L^3} - \frac{x_{F,i}^{(A)}}{r_{F,i}^3} \right) \\ &\quad + a_{X,L}^{(A)} - a_{X,F,i}^{(A)}, \\ \Delta \ddot{y}_{F,i}^{(A)} &= \ddot{y}_L^{(A)} - \ddot{y}_{F,i}^{(A)} = -2\omega_e \left(\dot{x}_L^{(A)} - \dot{x}_{F,i}^{(A)} \right) + \omega_e^2 \left(y_L^{(A)} - y_{F,i}^{(A)} \right) \\ &\quad - \mu_e \left(\frac{y_L^{(A)}}{r_L^3} - \frac{y_{F,i}^{(A)}}{r_{F,i}^3} \right) + a_{Y,L}^{(A)} - a_{Y,F,i}^{(A)}, \\ \Delta \ddot{z}_{F,i}^{(A)} &= \ddot{z}_L^{(A)} - \ddot{z}_{F,i}^{(A)} = -\mu_e \left(\frac{z_L^{(A)}}{r_L^3} - \frac{z_{F,i}^{(A)}}{r_{F,i}^3} \right) + a_{Z,L}^{(A)} - a_{Z,F,i}^{(A)}. \end{aligned} \quad (10)$$

When the spacecrafts in it are close to each other, the formation is $r_L \approx r_{F,i}$. Therefore, (9) can be simplified as

$$\begin{aligned} \Delta \ddot{x}_{F,i}^{(A)} &= 2\omega_e \Delta \dot{y}_{F,i}^{(A)} + \omega_e^2 \Delta x_{F,i}^{(A)} - \mu_e \frac{\Delta x_{F,i}^{(A)}}{r_L^3} + \Delta a_{X,F,i}^{(A)}, \\ \Delta \ddot{y}_{F,i}^{(A)} &= -2\omega_e \Delta \dot{x}_{F,i}^{(A)} + \omega_e^2 \Delta y_{F,i}^{(A)} - \mu_e \frac{\Delta y_{F,i}^{(A)}}{r_L^3} + \Delta a_{Y,F,i}^{(A)}, \\ \Delta \ddot{z}_{F,i}^{(A)} &= -\mu_e \frac{\Delta z_{F,i}^{(A)}}{r_L^3} + \Delta a_{Z,F,i}^{(A)}. \end{aligned} \quad (11)$$

By introducing the follower's relative state vector

$$\Delta \dot{\mathbf{X}}_{F,i}^{(A)} = \begin{bmatrix} \Delta \dot{\mathbf{r}}_{F,i}^{(A)} \\ \dot{m}_{F,i} \end{bmatrix}, \quad (12)$$

the state of the formation can be written as $\bar{\mathbf{X}}^{(A)} = [\mathbf{X}_L^{(A)}, \Delta \mathbf{X}_{F,1}^{(A)}, \dots, \Delta \mathbf{X}_{F,n}^{(A)}]$.

The center of the station-keeping box is located at an ideal displaced GEO, which is a fixed point in the frame (A). Its position is defined as $\mathbf{r}_{SKB}^{(A)} = [r_{GEO} + d_X, d_Y, d_Z]^T$, where the constants d_X, d_Y , and d_Z are position correction values and the r_{GEO} is the GEO orbit radius. To allow the spacecraft to move freely within the box, the station-keeping box is defined as $K = \{x, y, z \mid x \in [r_{GEO} + d_X - \rho_X, r_{GEO} + d_X + \rho_X], y \in [d_Y - \rho_Y, d_Y + \rho_Y], z \in [d_Z - \rho_Z, d_Z + \rho_Z]\}$ ($\rho_X, \rho_Y, \rho_Z \geq 0$), where ρ_X, ρ_Y , and ρ_Z are relaxing parameters.

The problem is solved with a numerical direct pseudospectral method implemented in the software tool PSOPT [19], which makes use of the automatic differentiation by

TABLE 2: Station-keeping box and relative distance parameters.

d_{\min} (km)	d_{\max} (km)	d_X (km)	d_Y (km)	d_Z (km)	ρ_X (km)	ρ_Y (km)	ρ_Z (km)
1	10	40	0	0	10	10	10

overloading in C++ (ADOL-C) library for the automatic differentiation of the objective, dynamics, constraint functions and the initial guess for the problem. We use the optimal trajectories and controls of strict formation-displaced GEO (results of Section 3) as the suboptimal initial guess for PSOPT, which allows the Gauss-pseudospectral algorithm to converge quickly and smoothly.

4.2. Results. In the test, the spacecraft's parameters are listed in Table 1 and the station-keeping box is defined in Table 2. According to Table 2, $d_{\min} = 1$ km, $d_{\max} = 10$ km, and the loosely degree is 9 km. The efficiency of solar sail is greatly affected by the sunlight direction which is the same as that of the Sun sail. Ignoring the minor differences between Sun-sail vector and the Sun-Earth vector in the simulation, we use the Sun-Earth vector rather than the Sun-sail vector to describe the sunlight direction. Considering the universal situations, we select the Sun-Earth vectors of winter solstice, spring equinox, summer solstice, and autumn equinox as the typical values. Unlike the strict formation, with the optimal trajectories of one orbital period (one day, see Figure 8), the relative distances between each two agents are not constant, which is always larger than d_{\min} and smaller than d_{\max} . Furthermore, the trajectories of the leader, follower 1, and follower 2 in a day are shown in Figure 9. It is obvious that the positions of all spacecrafts are restricted in the station-keeping box at any time. Because of the symmetry characteristic of the Sun-sail direction (see Figure 9), the shapes of spacecraft trajectories at winter solstice and summer solstice are symmetric (the same as the shapes at spring equinox and autumn equinox).

The mass consumption of each spacecraft is listed in Table 3, and the overall mass consumption (according to (9)) is listed in Table 4. With the station-keeping box and loosely formation, the mass consumption is greatly reduced both in the whole formation and each spacecraft. In the whole formation, the 2.805 kg, 3.022 kg, 2.808 kg, and 3.021 kg propellants are needed to maintain the strict formation at the ideal displaced GEOs for the winter solstice, spring equinox, summer solstice, and autumn equinox, respectively. By loosening the relative distance constraints and applying the station-keeping box, propellant mass is saved corresponding to the four seasons, 39.89% for winter solstice, 42.19% for spring equinox, 41.67% for summer solstice, and 42.04% for autumn equinox.

5. Conclusions

In this paper, with a hybrid (solar sail and solar electric propulsion, SEP) propulsion system, by inviting two concepts, the loosely relative distance constraints and the station-keeping box, a method to find the optimal trajectories of spacecraft formation for displaced geostationary orbits

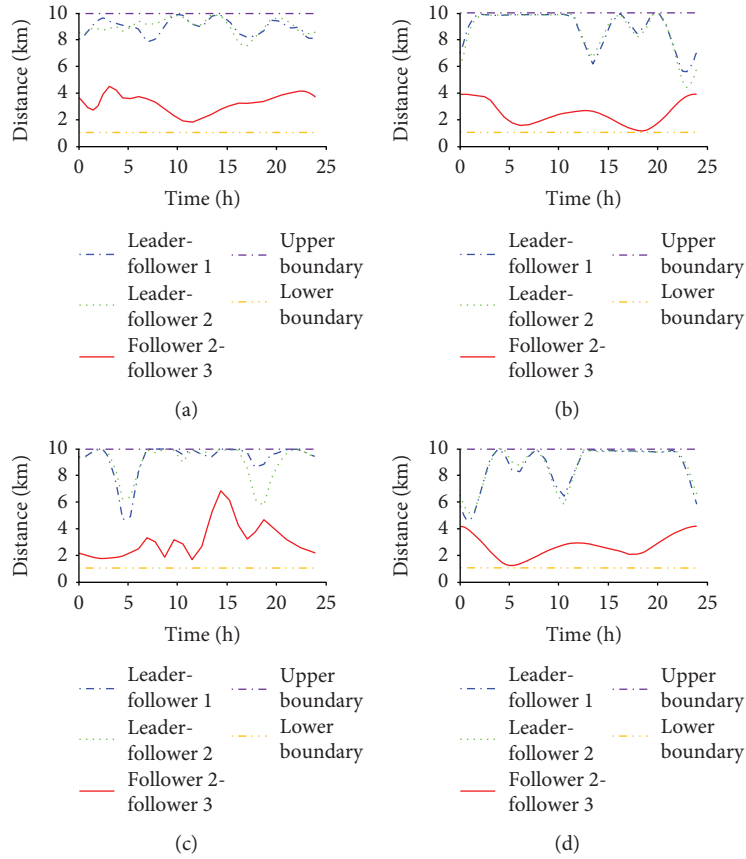


FIGURE 8: Loosely formation with station-keeping box: the relative distance of hybrid sail on (a) winter solstice, (b) spring equinox, (c) summer solstice, and (d) autumn equinox in the frame (A).

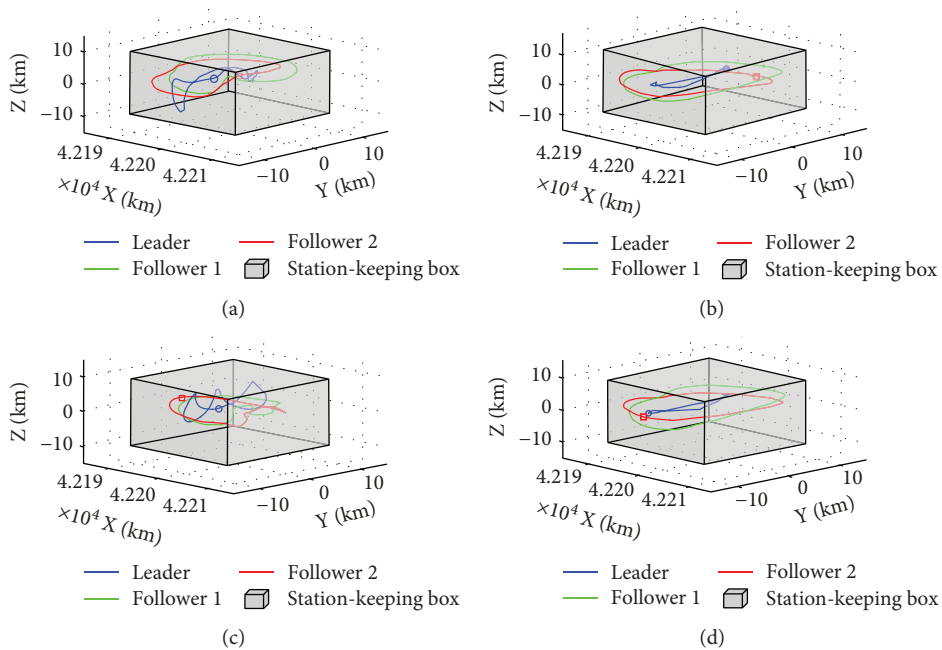


FIGURE 9: Loosely formation with station-keeping box: the trajectories of hybrid sail on (a) winter solstice, (b) spring equinox, (c) summer solstice, and (d) autumn equinox in the inertial frame.

TABLE 3: Mass consumption for each spacecraft after one day.

Time	Roles	Strict formation with ideal displaced GEO (kg)	Loosely formation with a station-keeping box (kg)	Mass saving (%)
Winter solstice	Leader	0.9155	0.4940	46.04%
	Follower 1	1.000	0.6220	37.80%
	Follower 2	0.8899	0.5700	31.99%
Spring equinox	Leader	1.077	0.5850	45.68%
	Follower 1	1.030	0.6160	40.19%
	Follower 2	0.9153	0.5460	40.34%
Summer solstice	Leader	0.9183	0.4550	50.45%
	Follower 1	1.000	0.6290	37.10%
	Follower 2	0.8894	0.5540	37.71%
Autumn equinox	Leader	1.076	0.5870	45.45%
	Follower 1	1.030	0.6180	40.00%
	Follower 2	0.9152	0.5460	40.34%

TABLE 4: Mass consumption for all spacecrafts after one day.

Time	Strict formation with ideal displaced GEO (kg)	Loosely formation with a station-keeping box (kg)	Mass saving (%)
Winter solstice	2.805	1.686	39.89%
Spring equinox	3.022	1.747	42.19%
Summer solstice	2.808	1.638	41.67%
Autumn equinox	3.021	1.751	42.04%

(GEOs) is introduced, which can be used as a solution to the congestion of the GEO. The hybrid sail spacecraft will consume less propellant to maintain the formation. For a $10 \times 10 \times 10 \text{ km}^3$ station-keeping box, which centers 40 km outside a real GEO and a 9 km loosely degree, propellant consumption saved 39.89%, 42.19%, 41.67%, and 42.04% for the winter solstice, spring equinox, summer solstice, and autumn equinox, respectively. The obvious mass saving shows that the station-keeping box and loosely relative distance constraints can improve the efficiency of the hybrid propellant system more efficiently than the ideal displaced GEO and strict relative distance formation. Besides, the optimization trajectories show that the station-keeping box can successfully restrict all the spacecrafts of the formation inside it. Furthermore, their relative distance is always larger than the lower boundary and smaller than the upper boundary.

Data Availability

All data in this manuscript are available for noncommercial applications upon request.

Conflicts of Interest

The authors declare that they have no conflicts of interest.

Acknowledgments

This research was jointly funded by China Natural Science Foundation (no. 61633008); Nature Science Foundation of Heilongjiang Province of China (no. F2017005); Fundamental Research Funds for the Central Universities, China (nos. HEUCFP201768 and HEUCFP201770); National Natural Science Fund (no. 11772185); Harbin Science and Technology Innovation Talent Youth Fund (no. 2015RQQXJ003); and Postdoctoral Science-Research Foundation (no. LBH-Q13042).

References

- [1] J. Heiligers, M. Ceriotti, C. R. McInnes, and J. D. Biggs, "Displaced geostationary orbit design using hybrid sail propulsion," *Journal of Guidance, Control, and Dynamics*, vol. 34, no. 6, pp. 1852–1866, 2011.
- [2] J. Heiligers, C. R. McInnes, J. D. Biggs, and M. Ceriotti, "Displaced geostationary orbits using hybrid low-thrust propulsion," *Acta Astronautica*, vol. 71, pp. 51–67, 2012.
- [3] R. McKay, M. Macdonald, J. Biggs, and C. McInnes, "Survey of highly non-Keplerian orbits with low-thrust propulsion," *Journal of Guidance, Control, and Dynamics*, vol. 34, no. 3, pp. 645–666, 2011.
- [4] L. Niccolai, A. A. Quarta, and G. Mengali, "Two-dimensional heliocentric dynamics approximation of an electric sail with fixed attitude," *Aerospace Science and Technology*, vol. 71, pp. 441–446, 2017.
- [5] M. Ceriotti, J. Heiligers, and C. R. McInnes, "Trajectory and spacecraft design for a pole-sitter mission," *Journal of Spacecraft and Rockets*, vol. 51, no. 1, pp. 311–326, 2014.
- [6] F. Dalla Vedova, H. Henrion, M. Leipold et al., "The Solar Sail Materials (SSM) project – status of activities," *Advances in Space Research*, vol. 48, no. 11, pp. 1922–1926, 2011.
- [7] T. Hirai, H. Yano, M. Fujii et al., "Data screening and reduction in interplanetary dust measurement by IKAROS-ALADDIN," *Advances in Space Research*, vol. 59, no. 6, pp. 1450–1459, 2017.
- [8] K. Newton, *NASA's First Solar Sail NanoSail-D Deploys in Low Earth Orbit*, NASA Marshall Space Flight Center, Huntsville, 2011, <http://www.nasa.gov/centers/marshall/news/news/releases/2011/11-010.html>.
- [9] L. Johnson, R. Young, N. Barnes, L. Friedman, V. Lappas, and C. McInnes, "Solar sails: technology and demonstration status," *International Journal of Aeronautical and Space Sciences*, vol. 13, no. 4, pp. 421–427, 2012.
- [10] J. Heiligers, M. Ceriotti, C. R. McInnes, and J. D. Biggs, "Design of optimal Earth pole-sitter transfers using low-thrust propulsion," *Acta Astronautica*, vol. 79, pp. 253–268, 2012.
- [11] J. Heiligers, M. Ceriotti, C. R. McInnes, and J. D. Biggs, "Design of optimal transfers between North and South Pole-sitter orbits," in *22nd AAS/AIAA Space Flight Mechanics Meeting*, Charleston, SC, USA, January-February 2012.
- [12] A. Reissner, N. Buldrini, B. Seifer, F. Plesescu, C. Scharlemann, and G. del AJ, "mN-FEEP thruster module design and preliminary performance testing," in *33rd International Electric Propulsion Conference*, Washington, 2013.
- [13] M. Walmsley, J. Heiligers, M. Ceriotti, and C. McInnes, "Optimal trajectories for planetary pole-sitter missions," *Journal of*

- Guidance, Control, and Dynamics*, vol. 39, no. 10, pp. 2461–2468, 2016.
- [14] G. Mengali and A. A. Quarta, “Trajectory design with hybrid low-thrust propulsion system,” *Journal of Guidance, Control, and Dynamics*, vol. 30, no. 2, pp. 419–426, 2007.
- [15] G. Mengali and A. A. Quarta, “Tradeoff performance of hybrid low-thrust propulsion system,” *Journal of Spacecraft and Rockets*, vol. 44, no. 6, pp. 1263–1270, 2007.
- [16] S. Baig and C. McInnes, “Artificial three-body equilibria for hybrid low-thrust propulsion,” *Journal of Guidance, Control, and Dynamics*, vol. 31, no. 6, pp. 1644–1655, 2008.
- [17] C. S. Arnot, C. R. McInnes, R. J. McKay, M. Macdonald, and J. Biggs, “Orbit period modulation for relative motion using continuous low thrust in the two-body and restricted three-body problems,” *Celestial Mechanics and Dynamical Astronomy*, vol. 130, no. 2, p. 12, 2018.
- [18] J. Heiligers, J. S. Parker, and M. Macdonald, “Novel solar-sail mission concepts for high-latitude Earth and lunar observation,” *Journal of Guidance, Control, and Dynamics*, vol. 41, no. 1, pp. 212–230, 2018.
- [19] V. M. Becerra, “Solving complex optimal control problems at no cost with PSOPT,” in *2010 IEEE International Symposium on Computer-Aided Control System Design*, pp. 1391–1396, Yokohama, Japan, Japan, September 2010.

